Applied Energy 386 (2025) 125594

Contents lists available at ScienceDirect

Applied Energy

journal homepage: www.elsevier.com/locate/apenergy

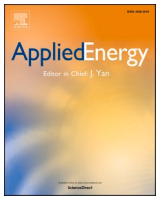

Degradation of commercial $Li_4Ti_5O_{12}$-based lithium-ion batteries under extremely fast cycling rates

Laisuo Su [a,b,*], Martin Z. Bazant [b,c,*], Alan Millner [d], Peng Bai [b,e,f,*]

[a] Department of Materials Science and Engineering, University of Texas at Dallas, Richardson, TX, 75080, USA
[b] Department of Chemical Engineering, Massachusetts Institute of Technology, Cambridge, MA 02139, USA
[c] Department of Mathematics, Massachusetts Institute of Technology, Cambridge, MA 02139, USA
[d] Lincoln Laboratory, Massachusetts Institute of Technology, Lexington, MA 02420, USA
[e] Department of Energy, Environmental and Chemical Engineering, Washington University in St. Louis, St. Louis, MO 63130, USA
[f] Institute of Materials Science and Engineering, Washington University in St. Louis, St. Louis, MO 63130, USA

HIGHLIGHTS

- A test protocol is proposed that can evaluate the aging of batteries on-board
- Two large-format commercial LTO batteries are tested with unique performance.
- Different aging mechanisms are uncovered in the two LTO batteries.
- A single-particle model is developed to predict battery aging behavior.

ARTICLE INFO

Keywords:
Lithium-ion battery
$Li_4Ti_5O_{12}$ anode
High C-rates
Aging mechanisms
Single particle model

ABSTRACT

$Li_4Ti_5O_{12}$ (LTO) is a promising anode material for lithium-ion batteries (LIBs) due to its good cycle stability, rate capability, and safety. The relatively high Li^+ intercalation plateau of about 1.55 V prevents the occurrence of lithium plating even at extremely high C-rates. In this study, we introduce a test protocol that can accurately evaluate the high-rate cycling performance of LTO-based LIBs. Two types of large-format commercial batteries are investigated, one with a capacity of 13 Ah (battery-A) and one with 3 Ah (battery-B). By incorporating two low-C-rate cycles every 50 high-C-rate cycles, we identify not only the overall capacity degradation but also the shifting state-of-charge range that the two types of batteries go through during cycling tests at various high C-rates (from 5C to 20C). Based on the uncovered mechanisms, a single-particle model is developed that can predict the aging behavior of the tested batteries at different C-rates. The study provides a simple onboard testing protocol to accurately evaluate the performance of LTO-based batteries.

1. Introduction

Lithium-ion batteries (LIBs) have become indispensable across various applications, including electric vehicles, mobile electronic devices, and grid energy storage systems. [1–3] Graphite dominates the anode market due to its low cost and solid overall electrochemical performance. However, LIBs with graphite anode cannot meet the requirements for specific applications, such as drones that require high power density to lift heavy loads. [4] Despite strategies such as structural engineering [5] and surface modification [6] have been developed to promote the fast-charging capability of a graphite anode, the high cost and difficulty in large-scale production limit their practical application. Compared to the state-of-the-art graphite anode and the high-energy density Si anode, $Li_4Ti_5O_{12}$ (LTO) has unique advantages in the aspect of cycle life, safety, and rate capability. [7]

The excellent cycle life of LTO comes from its "zero-strain" characteristic, with minimal volume change (~2 %) during Li^+ insertion/extraction due to the strong covalent bonding between Ti and O atoms. [8,9] This contrasts with silicon composites, which experience significant volume expansion (~300 %), leading to structural degradation over time. While graphite offers good cycle life under moderate conditions, its performance deteriorates rapidly under fast charging due to issues

* Corresponding author at: Department of Chemical Engineering, Massachusetts Institute of Technology, Cambridge, MA 02139, USA.
E-mail addresses: laisuo.su@utdallas.edu (L. Su), bazant@mit.edu (M.Z. Bazant), pbai@wustl.edu (P. Bai).

https://doi.org/10.1016/j.apenergy.2025.125594
Received 23 December 2024; Received in revised form 31 January 2025; Accepted 19 February 2025
Available online 27 February 2025

such as lithium plating. Moreover, LTO has a high Li^+ ion intercalation plateau of about 1.55 V (*vs.* Li/Li^+) that prevents electrolyte decomposition and Li dendrite formation, which is crucial for the safety of LIBs. [10] By comparison, graphite and silicon anodes have low operation voltage and suffer from Li dendrite formation under fast-charging or low-temperature operation. Additionally, strategies such as morphological regulation and hetero-atom doping have been developed to improve the ionic and electronic conductivity of LTO anode materials, [11–13] which promote the development of LTO-based LIBs with high-rate capabilities. [14]

Despite materials development suggesting that LTO is a very promising candidate for high-rate LIBs, the degradation of large-format commercial LTO-based batteries is yet to be fully investigated. [15] Moreover, the degradation mechanisms of LTO-based batteries are still debated in the literature. For example, Takami et al. tested a 3 Ah-class LTO/$LiMn_2O_4$ (LMO) battery for high-power applications at 10C for 30,000 cycles. [15] They found that the degradation of the LMO cathode is the major reason for the aging of LTO/LMO batteries, while the film growth on the surface of LTO is negligible during cycling. They also reported that the capacity fade of the battery is mainly dependent on the calendar life rather than the stress of charge/discharge cycling. Similar conclusions were made by Pasquier et al. who suggested the major cause of capacity fade of LTO/LMO battery is the impedance increase on the cathode caused by the formation of a resistive layer. [16] Svens et al. also found that the loss of positive electrode active material and loss of cyclable lithium are the major contributors to cycling capacity fading by studying a 3.1 Ah commercial LTO-based battery. [17] The tested battery also showed excellent calendar aging qualities with stable capacity and impedance over time. However, Belharouak et al. found a contradictory conclusion in a 2 Ah-class LTO/LMO battery during a storage test at high temperatures. [18] They found a coating on the LTO particles comprised of phosphorous, fluorine, and manganese that is primarily responsible for the capacity fading and impedance increase of the battery. It is, therefore, necessary to further investigate the aging behavior of LTO-based commercial batteries.

In this study, we developed a testing protocol that can help investigate the high C-rate cycling performance of large-format commercial LTO-based batteries. Two types of batteries were tested at various rates (from 5C to 20C) for up to 8000 cycles at 20 °C. The high-rate performance of the two types of batteries was compared and discussed. The incremental capacity analysis (ICA) method was applied to the cycling curves at a relatively slow C-rate, which could be used to uncover their aging mechanisms. A single-particle aging model was developed based on the obtained aging mechanism that could accurately predict the degradation behavior of these batteries. By shedding light on the high-rate performance and aging mechanisms of commercial LTO batteries, this work provides critical insights into their limitations and guides the evaluation and onboard testing of high-power LTO batteries.

2. Experiment

2.1. Battery information

Table 1 lists the information of the two commercial batteries investigated in this study, which were provided by an industry partner. The battery-A has a 13 Ah nominal capacity, and the battery-B has a 3 Ah nominal capacity, which was used to determine the currents at different C-rates for both rate tests and cycling tests. The anode material for both types is LTO. The cathode material for battery-A is LMO, while that for battery-B is protected from disclosure. The most possible cathode material for battery-B is a transition metal layered oxide such as $LiNi_xMn_yCo_zO_2$ (NMC) according to its charge and discharge curves and their ICA curves, which will be explained in the later section of the paper. The voltage ranges were chosen based on the information provided by vendors. Other information about the two types of batteries such as electrode thickness and battery structure are protected from disclosure, although they have a significant impact on the electrochemical performance of the battery.

Table 1
Basic information of the two types of tested LTO-based batteries.

Battery Type	Chemistry		Capacity	Voltage range (V)
	Anode	Cathode	(Ah)	
battery-A	$Li_4Ti_5O_{12}$	$LiMn_2O_4$	13	1.5–2.8
battery-B	$Li_4Ti_5O_{12}$	$LiNi_xMn_yCo_zO_2$*	3	1.8–2.8

*Note: The cathode material of battery-B is not provided by the vendor, and the composition is based on our understanding from tested data.

2.2. Cycling tests

A cycling protocol was developed in this study to evaluate the performance of the two LTO-based batteries during cycling at high rates. For the high-rate long-term cycling testing, batteries were cycled at a standard constant current charge/discharge (CC/CC) using Arin HC-5 in an environmental chamber (SPX model TJR-A-F4). Batteries were charged at a constant current until they reached the charge cut-off voltages, followed by a constant current discharge process to the discharge cut-off voltages. The cut-off voltages are listed in Table 1 for the two types of batteries. Three different cycling C-rates were applied for both types of batteries, including 5C/5C, 10C/10C, 15C/15C for battery-A, and 5C/5C, 10C/10C, 20C/20C for battery-B.

After every 50 cycles, two 1C/1C cycles were implemented to help evaluate the electrochemical performance of the two types of batteries. The relatively slow C-rate can diminish the capacity loss due to dynamic effects such as concentration depletion occurring at the microscopic level. The actual cycling state-of-charge (SOC) ranges during high-rate cycling can be derived with the help of these 1C/1C cycling. Moreover, the degradation mechanisms of batteries can also be analyzed from the 1C/1C cycling curves.

Fig. 1a shows an example of the test profile of battery-A being tested at 5C/5C. The ambient temperature was controlled to 20 °C by a temperature chamber during the experiment, and the surface temperature of the batteries was recorded by a thermocouple. The decision to maintain temperature control at 20 °C is based on its relevance to real-world operating conditions, where ambient room temperature is a common baseline for evaluating battery performance. This temperature minimizes external thermal effects, ensuring that the observed performance and degradation behaviors are intrinsic to the batteries and not influenced by extreme thermal conditions. Fig. 1b shows that the temperature increase for battery-A at the 5C/5C test was up to 7 °C. The temperature increase could be even higher at a higher testing C-rate. Thus, a six-minute relaxation step was introduced after each charge and discharge step to avoid the continuous accumulation of heat inside the battery.

3. Results and discussion

3.1. The rate performance and actual SOC ranges of batteries during cycling

Fig. 2a, b compares the charge and discharge curves at different C-rates of the two types of batteries. These curves show different shapes, especially at the end of charge/discharge, which could be from different cathode materials used in these two batteries. The rate test results suggest that battery-A is affected more by the cycling rate. The capacities that the battery-A can output are 84 %, 56 %, and 19 % of the 1C nominal capacity at 5C, 10C, and 15C, respectively. By comparison, the battery-B retains 89 %, 80 %, and 73 % of its 1C nominal capacity at 5C, 10C, and 20C, respectively. Thus, the high-rate performance of battery-B is better than battery-A.

A battery is under-charged and under-discharged when being tested

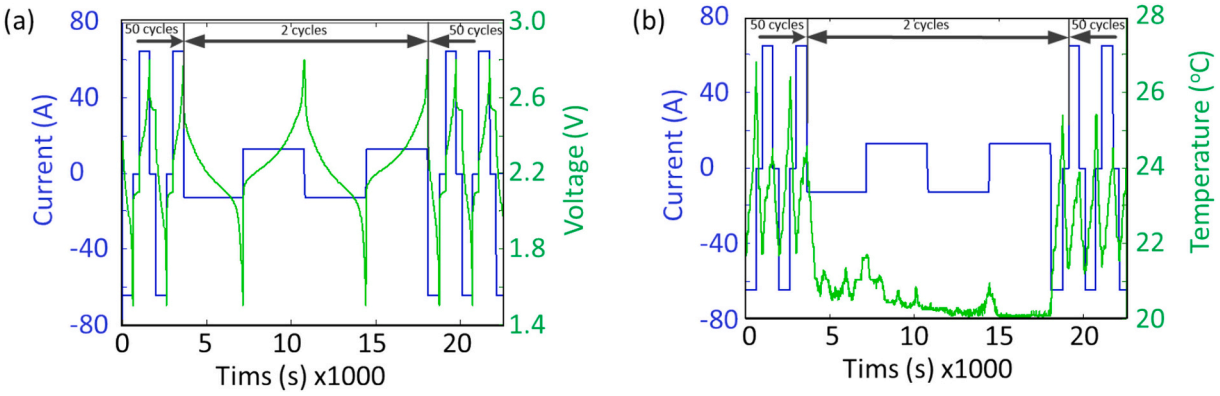

Fig. 1. The test protocol for commercial LTO-based batteries. (a) The current and voltage profiles of battery-A during a cycling test. Two 1C/1C cycles were conducted for every 50 cycles. (b) The current and temperature profiles of the battery during testing. The temperature is maintained at around 20 °C during the 1C/1C cycles.

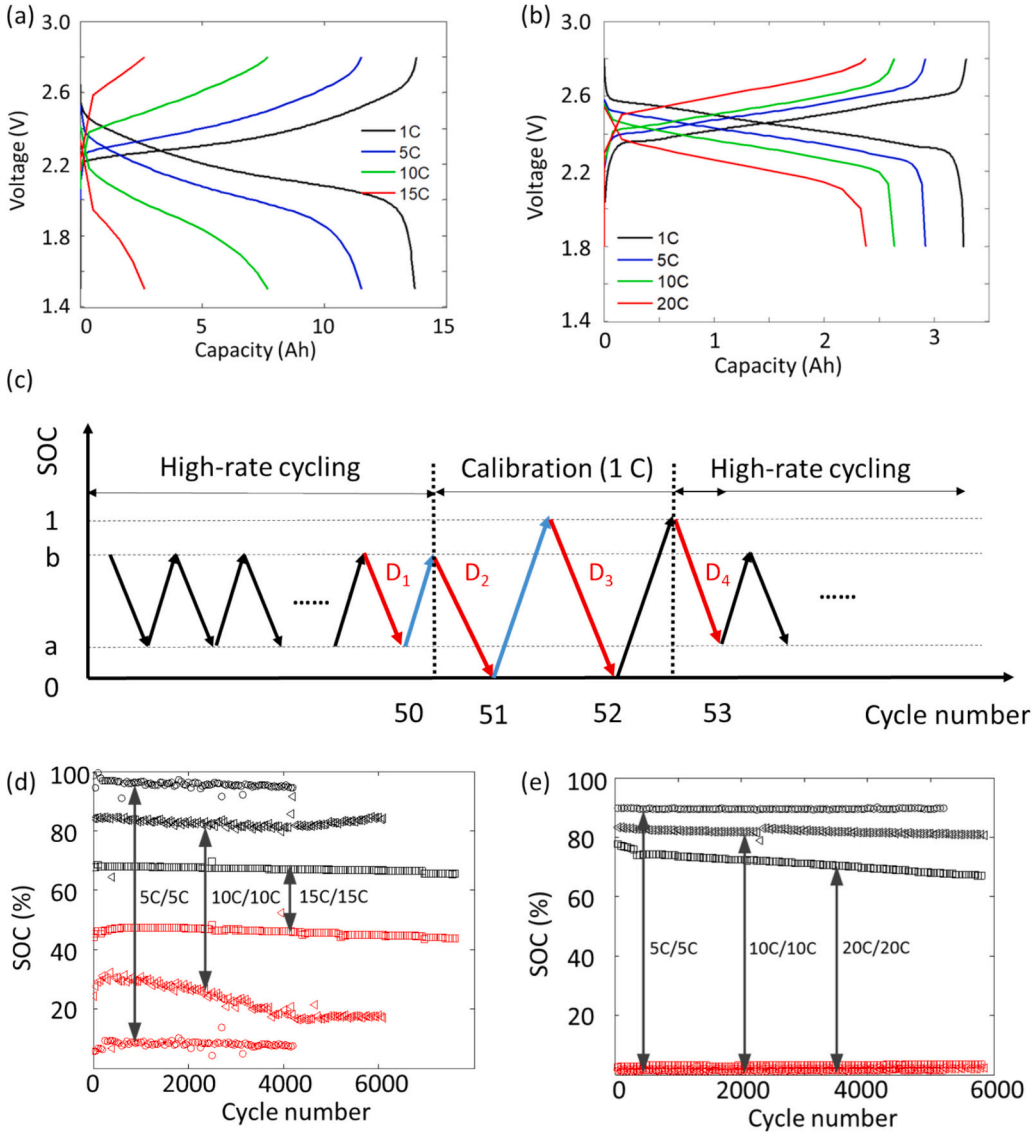

Fig. 2. Analysis of the cycling test at different C-rates. (a, b) Charge and discharge curves at different cycling rates for (a) battery-A and (b) battery-B. (c) A schematic that shows the actual SOC ranges at different C-rates during cycling. (d, e) The calculated SOC intervals at different C-rates during testing for (d) battery-A and (e) battery-B.

at a high C-rate because of the large overpotential generated within the battery. In this study, we define that the battery reaches 100 % SOC during charging at 1C and returns to 0 % SOC during discharge at 1C. At a high C-rate, the battery is cycling within the SOC interval of [a, b], where 0 % < a < b < 100 %. The exact values of a and b depend on the battery type, cycling rate, and the status of the battery. Fig. 2c shows a schematic of the SOC ranges that a battery went through during testing at a high C-rate. Four different discharge capacities (D_1, D_2, D_3, and D_4) are labeled out in Fig. 2c, and the values of a and b can be calculated based on the formula (1) and (2).

$$a = \frac{D_3 - D_4}{D_3} = b - \frac{D_1}{D_3} \tag{1}$$

$$b = 1 - \frac{D_3 - D_2}{D_3} \tag{2}$$

Fig. 2d compares SOC intervals at different cycling rates of the battery-A. The results suggest that the battery was under-charge and under-discharge at high C-rates. The degree of under-charge and under-discharge levels increased dramatically with the C-rate. At the 15C/15C test, the battery-A was cycled only between 45 % - 65 % SOC. By comparison, the SOC interval profile in Fig. 2e suggests that battery-B had much better capacity retention at a high C-rate. The battery could always reach ~0 % SOC regardless of the cycling C-rate. However, the C-rate affected the degree of under-charge. Thus, the source that limits the high-rate performance of battery-B is the charging process.

The results can be related to the charge and discharge curves as shown in Fig. 2a, b. When a battery is near to being fully charged or discharged, a very steep curve that is almost perpendicular to the x-axis, would appear. This phenomenon is not fully understood, which could be from the lack of Li^+ ion in one of the electrodes, causing high diffusion resistance and leading to high overpotential. Fig. 2a shows both the charge and discharge curves change to be vertical at the end of cycling in the 1C/1C test. At high C-rates, the vertical parts disappear for both charge and discharge curves, indicating the under-charge and under-discharge states of battery-A. By comparison, Fig. 2b displays that the vertical parts of the discharge curves remain, while they disappear in the charge curves at high C-rates, indicating that battery-B could be fully discharged but could not be fully charged at high C-rates.

The different SOC ranges for the two types of batteries under high C-rates could be attributable to multiple factors, including their material and design features. While the cathode material is a significant contributor to the SOC range, other factors, such as the electrolyte formulation, electrode architecture, and overall cell design, also play critical roles. Specifically, battery-B may utilize cathode material with higher ionic conductivity or a more robust structure that allows for efficient Li^+ intercalation and de-intercalation over a wider SOC range. Additionally, the electrolyte composition in battery-B could be optimized to reduce resistance and enhance Li^+ transport at high C-rates. Differences in electrode porosity, thickness, and the ratio of binder to conductive agent could also affect ionic and electronic pathways, enabling more uniform utilization of the active materials.

3.2. Capacity fading of LTO-based batteries during high-rate cycling

The two types of batteries were continuously cycled at three different C-rates for thousands of cycles. Fig. 3 compares the cycling performance at all the tested conditions. Fig. 3a compares the cycling performance of battery-A at three different C-rates. The capacity degradation of battery-A fluctuates at 5C and 10C, which could be from the temperature variations during cycling. Although batteries were tested in an environmental chamber, the temperature of a battery still increases during cycling, which can influence electrolyte conductivity, reaction kinetics, and overall cell performance. Localized heating may temporarily

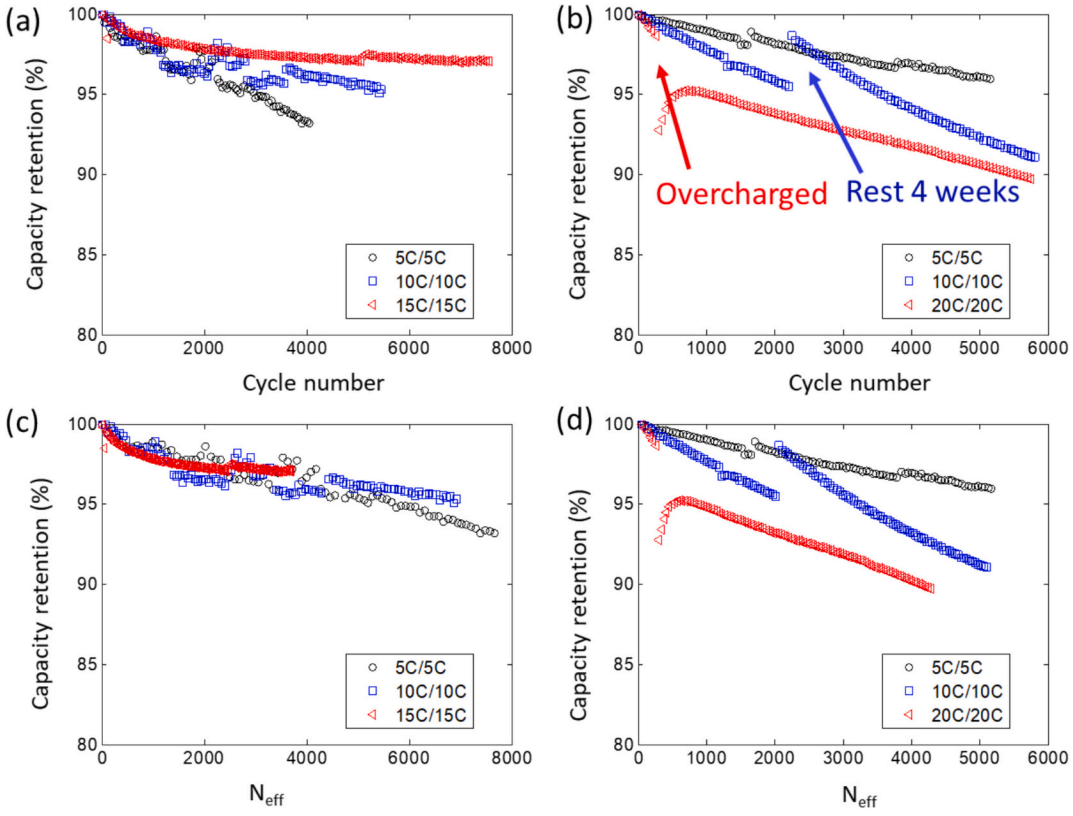

Fig. 3. The cycling performance of two LTO-based commercial batteries at various C-rates. (a, b) The evolution of capacity retention with respect to cycle number for (a) battery-A and (b) battery-B. (c, d) The evolution of capacity retention of the two types of batteries with respect to the effective cycle number (N_{eff}) which is defined in this study for a fair comparison among different C-rates.

enhance ion transport, while cooling periods could reduce capacity, leading to fluctuations. In addition, variations in lithium-ion diffusion and migration within the electrolyte can lead to intermittent changes in capacity, particularly at high charge/discharge rates. Localized concentration gradients may result in non-uniform lithiation/de-lithiation, causing fluctuations in capacity retention, which has been reported in the literature. [19] Nevertheless, these factors do not impact the overall trend of capacity degradation of battery-A. The result suggests that battery-A has better capacity retention when being cycled at a higher C-rate. The capacity fading rate is the slowest at 15C/15C, while is the fastest at 5C/5C. Such a finding is contradictory to our conventional understanding that a higher current generally leads to faster capacity fading of a battery. [3] The reason for such phenomena is that battery-A went through different SOC ranges when being tested at different C-rates (Fig. 2d). Thus, the cycle number is not an appropriate index for comparing the aging of the battery at different C-rates.

Other indexes such as Ah-throughput and energy-throughput have been used. [20] However, the nominal capacity of battery-A (13 Ah) is much larger than battery-B (3 Ah), and these indexes cannot be used directly to have a fair comparison of the two batteries. We proposed an index N_{eff}, namely "effective cycle number", to normalize the Ah-throughput of a battery by its normal capacity. The value of N_{eff} can be calculated from Eq. (3). The obtained N_{eff} represents the number of full charge/discharge cycles that a battery goes through during cycling. Fig. 3c compares the capacity fading of battery-A at the three cycling C-rates using N_{eff} as the index. The result suggests that the capacity fading rate is not significantly affected by the testing C-rate. More than 90 % of capacity is retained after over 8000 cycles for all the testing C-rates.

$$N_{eff} = \frac{Ah_{throughput}}{2 \cdot Cap_{nominal}} \tag{3}$$

where $Ah_{throughput}$ is the capacity (in the unit of Ah) that a battery has gone through, and $Cap_{nominal}$ is the nominal capacity, which is 13 Ah for the battery-A and 3 Ah for the battery-B.

Fig. 3b displays the cycling performance of battery-B at different C-rates. It should be mentioned that there are some abnormal issues during the tests for battery-B. At the 10C/10C test, the battery was unintentionally stopped and rested at room temperature for four weeks after the 2391st cycle. After the rest period, the battery showed a much higher capacity in the beginning when it was back to the cycling test. A similar capacity recovery phenomenon after resting has been reported in the literature. [21] For the 20C/20C test, the battery was over-charged to 3.6 V (instead of the normal 2.8 V) at the 340th cycle due to the software malfunction. The over-charging may lead to side reactions, such as electrolyte decomposition, gas evolution, or structural changes in the electrode materials, which could affect long-term battery performance. These mechanisms can be correlated to the much lower capacity after the happening of overcharging. A self-healing process was discovered for battery-B after the unexpected over-charge, which warrants further investigation. Thus, only the initial section without the unexpected resting or overcharging of the cycling profiles of the 10C/10 and the 20C/20C cycling tests were used to evaluate the performance of battery-B at these C-rates. Fig. 3d applied the N_{eff} as the index to compare the capacity fading of battery-B at the three cycling C-rates. Different from the performance of the battery-A shown in Fig. 3c, the C-rate has a significant impact on the capacity fading rate of the battery-B, and a higher C-rate leads to faster capacity fading. A linear extrapolation of the cycling curves suggests that the battery-B can be cycled for around 22,000, 8000, and 3000 times, respectively, at the 5C/5C, 10C/10C, and 20C/20C when its capacity decreases to 80 % of its nominal capacity.

3.3. Capacity fading mechanisms of LTO-based batteries

The different degradation behavior of battery-A and battery-B suggests that they have different capacity fading mechanisms. However, the vendors did not permit us to disassemble these batteries for materials characterizations of the electrodes or harvest the electrodes to fabricate Li metal half cells for electrochemical testing. To uncover the mechanism without opening these batteries, the discharge curves at 1C rate during the calibration process were investigated through ICA, which is a powerful technique that has been developed to study the degradation mechanisms of batteries. [22,23] It can convert plateaus in a cycle curve to ICA peaks by dividing the capacity by voltage (dQ/dV), and each ICA peak represents a phase transition process of the two electrodes during lithiation/de-lithiation. Generally, a slow C-rate such as C/25 is required for ICA analysis to eliminate the kinetic impact. However, this extremely low C-rate test is hard to implement with an onboard battery management system for electric vehicles. In this study, we nonetheless adopt this method but use a relatively higher current at 1C during the calibration test.

Fig. 4 shows the analysis of the capacity fading of battery-A during cycling. As all the batteries show similar aging modes at the three C-rates (5C, 10C, and 15C), the battery under the 5C/5C cycling test was chosen for the ICA analysis because it went through the longest cycle (Fig. 3c). Fig. 4a displays the ICA curves of the battery-A after various cycles. Two peaks can be distinguished from the curve, and they are labeled as 1 and 2. We assume the LTO anode has a steady voltage profile during the cycling, [24] and thus the ICA peaks contain the information of the cathode evolution during cycling. The area under each ICA peak is related to the amount of cathode active material (CAM) that is involved in a lithiation process causing a two-phase coexistence. When one phase of the CAM is converted to the other phase during lithiation, the potential of the cathode will change dramatically, leading to the disappearance of an ICA peak. Thus, the two ICA peaks suggest that there are two two-phase transition regions for the CAM during its lithiation.

Here, we assume the LTO anode does not degrade during cycling, [15–17] and the capacity fading is mainly caused by the degradation of the CAM during cycling. Based on such assumption, the evolution of the two ICA peaks and their areas can be correlated to the two major degradation mechanisms, which are the loss of lithium inventory (LLI) and the loss of active materials (LAM) of the cathode. The LLI could be from the side reactions between electrolytes and electrodes that consume the total amount of available active Li^+ used to store energy. The LAM of the cathode can cause the decrease of areas of both peak 1 and peak 2. By comparison, the LLI only affects the area of peak 1 because the battery is under-charged at the fully charged status when the amount of Li^+ ion is not sufficient. If the LLI is the only degradation mechanism, the area of peak 2 will be affected after peak 1 disappears. To quantify the area under each ICA peak, the membership function (MF) is used by reference to fuzzy logic, as shown in Fig. 4b. [25,26] A linear function was chosen within the overlap region between the two ICA peaks to simplify the calculation, which is caused by the non-steady state of the cathode during discharging. The area under each ICA peak can be calculated from the formula (4) and (5).

$$Q_1 = \int_{V_{min}}^{V_{max}} \mu_1 \cdot \frac{dQ}{dV} dV \tag{4}$$

$$Q_2 = \int_{V_{min}}^{V_{max}} \mu_2 \cdot \frac{dQ}{dV} dV \tag{5}$$

The discharge curve at cycle 50 was considered as the initial condition, and the two peaks at cycle 50 were used to normalize the peak areas in other cycles to highlight the change of the peak areas during cycling. Fig. 4c compares the evolution of the normalized peak areas for both peak 1 (Q1) and peak 2 (Q2). Overall, the peak area under the second peak (Q2) shows much less change compared to Q1 during cycling. In the first 3000 cycles, Q1 gradually decreases while there is negligible change in Q2, suggesting that the capacity fading is mainly

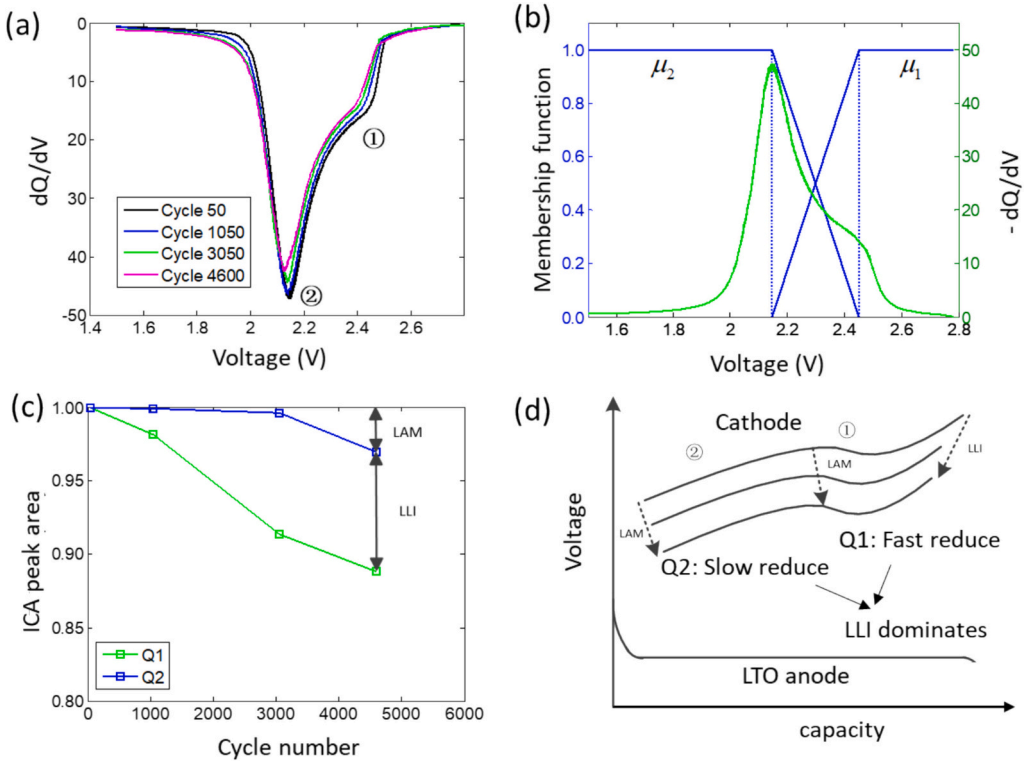

Fig. 4. Analysis of capacity fading mechanisms of the battery-A during cycling. (a) The ICA analysis of the 1C discharge curves of the battery after various cycles. (b) Quantifying the area under each ICA peak using the fuzzy logic method. (c) The evolution of the ICA peak area normalized to cycle 50 (Q1 and Q2). (d) A schematic to demonstrate the two fading mechanisms and how they affect the voltage profile of the cathode electrode.

caused by the LLI in this period. The LLI can be from the formation of passivating films on the surface of both electrodes. [16] After 4600 cycles, Q2 shows around 3 % decrease that can be attributed to the LAM. The degradation mechanisms are schematically summarized in Fig. 4d, where the LLI leads to a reduced SOC level when a battery is fully charged, while the LAM leads to a shrinkage of the discharge curve.

The degradation mechanisms of LAM could be from (1) cathode degradation: the cathode material undergoes phase changes and microstructural deterioration over thousands of cycles. These changes reduce the number of active lithium storage sites, directly contributing to the loss of active material. (2) LTO anode aging: while the LTO anode is known for its structural stability, prolonged high-rate cycling can lead to minor mechanical stress and gradual detachment of the electrode particles from the conductive network. This results in reduced utilization of active material. However, the exact mechanisms for the LAM are hard to obtain without material characterizations, which is beyond the scope of this study.

To uncover the degradation mechanisms of battery-B during high C-rate cycling, a similar ICA analysis was conducted. The 10C/10C cycling test result was selected for analysis because the battery showed a greater degree of capacity fading than the one with the 5C/5C cycling test. The battery under 20C/20C had an abnormal over-charge which may affect the following degradation mechanisms and thus was not suitable for the ICA analysis.

Fig. 5a shows the ICA curves of battery-B at different numbers of cycles. Three ICA peaks can be identified that are labeled as 1, 2, 3 in the figure. During cycling, the locations of the three peaks shift to lower voltages, indicating a gradually increased impedance within the battery that leads to increased overpotential. Moreover, the intensities of all three peaks decrease simultaneously during cycling. We did not apply the Fuzzy logic MF to quantify the area under each peak. A simple linear MF may lead to misleading conclusions due to the increased number of

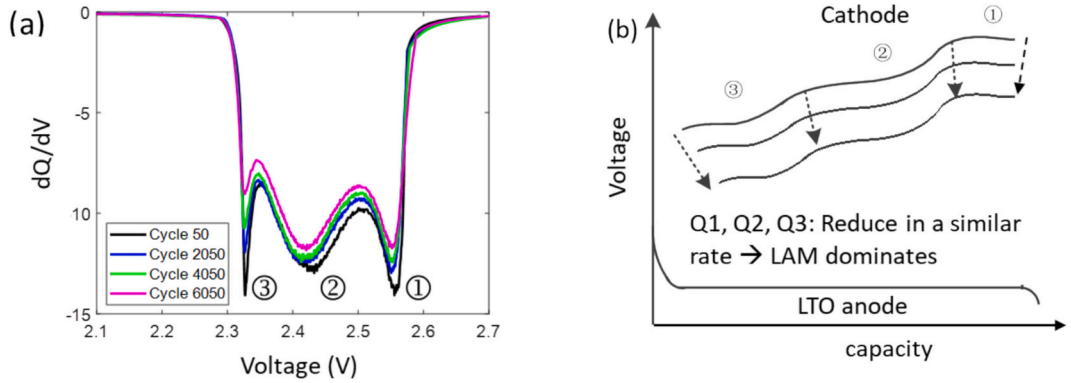

Fig. 5. Analysis of capacity fading mechanisms of the battery-B during cycling. (a) The ICA analysis of the 1C discharge curves of the battery after various cycles. (b) A schematic to demonstrate the major fading mechanism of LAM and how it affects the voltage profile of the cathode electrode.

peaks (three instead of two for the battery-A) and the significant overlapping among them. A qualitative analysis of the ICA curve suggests that LAM is the major capacity fading mechanism, which can lead to a proportional decrease in the areas of all the ICA peaks. Fig. 5b displays the proposed degradation mechanism of battery-B. The LTO anode does not change much during cycling, while the length of the charge curve from the cathode gradually decreases due to the LAM.

The two different degradation mechanisms for the two types of batteries obtained from the ICA analysis can be correlated to their different cathode materials. Battery-A, which utilizes LMO as the cathode, primarily suffers from **LLI (**Fig. 4**).** This degradation mechanism is often linked to side reactions at the electrolyte-electrode interface, such as electrolyte decomposition and the formation of a thick SEI on the anode, which trap lithium ions and reduce the amount available for intercalation/de-intercalation. Additionally, manganese dissolution from LMO into the electrolyte can accelerate LLI by inducing irreversible capacity loss. In contrast, battery-B, which employs an NMC cathode, experiences LAM as the dominant degradation mechanism (Fig. 5). This is likely due to structural degradation of the NMC particles, including microcracking, transition metal dissolution, and phase transformations, which progressively reduce the amount of electrochemically active material contributing to capacity. The more pronounced LAM in battery-B suggests that cathode degradation plays a more critical role in its performance fading compared to lithium inventory loss. These findings emphasize the importance of tailoring electrode materials and cell designs to mitigate specific degradation mechanisms for long-term battery performance.

3.4. Single-particle aging model to predict battery aging behavior

The capacity fading mechanism of the battery-A is dominated by the LLI, which could be from the formation of passivation layers on the surface of both the cathode and anode. The theory of SEI formation has been extensively studied and different models have been proposed for graphite anode. [27–29] However, little modeling work has been done for LTO-based batteries to predict their capacity fading. Here, we developed a single particle model based on a few assumptions to study the capacity fading of the battery-A.

Despite the passivation layers form on both sides of the electrodes, we assume that the solid-electrolyte interphase (SEI) formed on the LTO anode side is the dominant factor because the cathode-electrolyte interphase layer is usually very thin. [30] The evolution of the thickness of SEI (s) can be described by Eq. (6). [28]

$$\frac{ds}{dt} = \frac{Jm}{\rho A} \tag{6}$$

where J is the rate of side reactions, m is the mass of SEI formed by a single reaction, ρ is the density of SEI, and A is the surface area of anode material that side reaction could occur. The side reaction rate can be described by Eq. (7) based on the first-order reaction assumption.

$$J = kA(\mathrm{c} - \Delta c) \tag{7}$$

where Δc is the concentration difference of reaction species between the outside and the inside of the SEI. The Δc can be solved based on Fick's first law.

$$\Delta c = \frac{Js}{AD} \tag{8}$$

where D is the diffusivity through the SEI of the species that reacts with lithium to form SEI. From Eqs. (6)–(8), the increase rate of the thickness of SEI can be derived

$$\frac{ds}{dt} = \frac{kcDm}{\rho(D + ks)} \tag{9}$$

The capacity loss of a battery is proportional to SEI thickness which can be correlated to the loss of lithium inventory within the battery.

$$Q_{loss} = \frac{sA\rho}{m}\frac{Ne}{t_0} \tag{10}$$

where N is Avogadro's number (6.02×10^{23} mol^{-1}), e is the electronic charge on an electron (1.602×10^{-19}C), and t_0 is the constant that equals 3600 s·h^{-1}. The capacity fade rate can be calculated from Eqs. (9) and (10)

$$\frac{dQ}{dt} = -\frac{kcDA^2\rho g^2}{\rho DAg + km(Q_0 - Q)} \tag{11}$$

where $g = Ne/t_0$, and the value of g is 26.79 Ah mol^{-1}.

In Eq. (11), k and D need to be fitted in our model. Since the species of SEI is unclear, we assume that c is 1 M, which is an arbitrary value because we do not have the information on electrolytes used in the battery. A is calculated based on battery capacity and coating parameters. ρ and m are two SEI characteristics, lithium fluoride is chosen as a typical SEI component, and its molar mass is 26 g mol^{-1} and density is 2.6 g·cm^{-3}.

The diffusion coefficient D depends on temperature, and follows the Arrhenius law, as shown in Eq. (12). [28] Although the temperature of the battery is not constant during cycling, we included a rest step to minimize the change. As the variation of the temperature is much smaller than E_a/k_B, the Eq. (12) can be simplified to Eq. (13), where the derivation process is shown in Appendix A for reference.

$$D \propto exp\left(-\frac{E_a}{k_B T}\right) \tag{12}$$

$$D = D_0 exp(\alpha I) \tag{13}$$

Fig. 6a fits the single-particle model with tested results in the 5C/5C and the 15C/15C cycling tests. The parameter k is 1.0×10^{-11} s^{-1} for both conditions. The value is lower than the reaction rate on the surface of graphite reported in some research, such as 10^{-3} - 10^{-7} s^{-1}. [31] The small k value explains the long lifespan of LTO-based batteries. The parameter D is 5.0×10^{-21} m^2 s^{-1} for the 5C/5C condition, while is 2×10^{-20} m^2 s^{-1} for the 15C/15C condition. The general Li^+ diffusion coefficient values for the SEI formed on graphite anode is 10^{-11} - 10^{-18} m^2 s^{-1}. [31] However, the parameter D calculated here represents the diffusion coefficient of electrolyte solvents or reactive species through SEI, which is usually not reported in the literature. Moreover, the exact composition of the electrolyte of battery-A is not disclosed by the vendor. Thus, it is hard to evaluate the accuracy of the D values fitted from the experimental data.

Combining the formula (13) with the D values at the 5C/5C and the 15C/15C tests, we calculated the D value at the 10C/10C test to be 1.0×10^{-20} m^2 s^{-1}. The k value is the same for all the test conditions. Based on these parameters, the capacity fading of battery-An under 10C/10C cycling was predicted. Fig. 6b compares the predicted capacity fading that shows a good match with the measured performance, indicating the applicability of the developed single-particle model in predicting the degradation of battery-A at other cycling conditions.

It is worth noting that the single-particle aging model developed in this study effectively captures the observed degradation trends of LTO-based batteries under high C-rate cycling. While the model supports the hypothesis that SEI formation significantly contributes to the observed capacity fading, it remains an indirect method of assessing degradation mechanisms. Direct material characterization, such as post-mortem analysis of the electrode surfaces and SEI composition, would be necessary to validate the model's assumptions and provide definitive evidence of the role of SEI formation. Future studies could integrate techniques such as X-ray photoelectron spectroscopy, transmission electron microscopy, or nuclear magnetic resonance spectroscopy to confirm the relationship between SEI properties and battery aging. Including material analysis would strengthen the understanding of

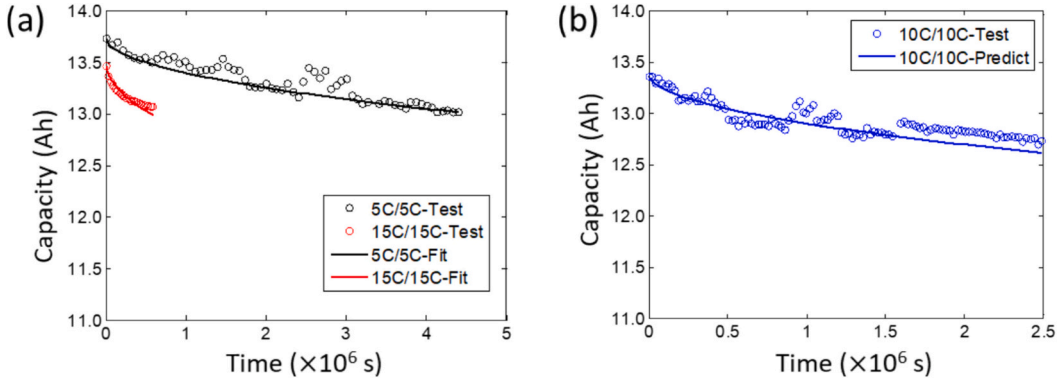

Fig. 6. Validation of the single particle model to predict the capacity fading of the battery-A. (a) Fitted results of the battery under the 5C/5C and the 15C/15C cycling tests. (b) Predicted results of the battery under the 10C/10C cycling test.

degradation mechanisms and further enhance the predictive capability of the model.

4. Conclusion

In this study, we developed a simple test protocol that can be used to evaluate the degradation behavior of LTO-based batteries during high-rate cycling tests. By applying such a test protocol, we uncovered the rate capability and degradation behavior of two large-format commercial LTO-based LIBs under high C-rate cycling. Despite battery-A and battery-B having the same LTO anode, their rate performance and cycling stability are quite different. The battery-B can always be fully discharged to almost 0 % SOC even at 20C, while the battery-A is running within a limited SOC range of around 45 % - 65 % at 15C/15C. These differences can be attributed to many other factors such as cathode material, electrode composition (ratio of binder and conductive agent), electrode thickness and porosity, and electrolyte composition.

Both LTO-based batteries showed excellent cycling stability with thousands of cycles with less than 10 % capacity fading. However, different degradation patterns are found for the two types of batteries. The capacity fading rate of the battery-A is not affected by the C-rate. All the batteries can reach over 10,000 effective cycles with over 90 % of capacity retention. However, the C-rate significantly affects the capacity fading rate of battery-B, with a higher C-rate leading to faster capacity fading. The different degradation behaviors can be correlated to their different aging mechanisms that are uncovered based on the analysis of 1C/1C cycling curves. The degradation mechanisms of battery-A are dominated by the LLI, while they are dominated by the LAM for battery-B. The different aging mechanisms could be from many factors such as cathode material, electrode composition, electrode thickness and porosity, and electrolyte composition. We further developed a single-particle model that can predict their degradation behavior at different cycling conditions.

In summary, we obtain plenty of information on the electrochemical performance and aging mechanisms of LTO-based batteries by implementing two continuous 1C/1C cycling tests in between high-rate testing. Such a test protocol can be implemented onboard in practical applications to help understand the status of these LTO-based batteries. In addition, the method presented in this study can also be extended to commercial LIBs with anodes such as widely used graphite and silicon. The approach can provide valuable insights into the intercalation and de-intercalation dynamics, as well as the evolution of SEI under varying cycling conditions. This could lead to a better understanding of the mechanisms of capacity fading and the impact of high-rate cycling on the electrochemical performance of commercial batteries.

CRediT authorship contribution statement

Laisuo Su: Writing – review & editing, Writing – original draft, Visualization, Investigation, Formal analysis. **Martin Z. Bazant:** Writing – review & editing, Supervision, Resources, Project administration, Methodology, Investigation, Funding acquisition, Conceptualization. **Alan Millner:** Supervision, Resources, Methodology. **Peng Bai:** Writing – review & editing, Validation, Supervision, Methodology, Investigation, Data curation, Conceptualization.

Declaration of competing interest

The authors declare that they have no known competing financial interests or personal relationships that could have appeared to influence the work reported in this paper.

Acknowledgments

This work was partially supported by the MIT Lincoln Laboratory. L. S. acknowledges the New Faculty startup funding provided by the University of Texas at Dallas. P.B. acknowledges the support of an NSF grant (No. 2044932).

Appendix A. Appendix

Relation between diffusion coefficient (D) and current (I).

The temperature of the tested battery is increased during cycling, which can be correlated to the current through Eq. (14).

$$\Delta T = \beta \cdot I \tag{14}$$

We assume the temperature increase is much smaller than room temperature, which is itself much smaller than E_a/k_B

$$\Delta T \ll T \ll Ea/k_B \tag{15}$$

D follows the Arrhenius's law

$$D = Aexp\left(-\frac{E_a}{k_B T}\right) = Aexp\left(-\frac{B}{T_0 + \Delta T}\right) = Aexp\left(-\frac{B}{T_0}\cdot\frac{1}{1 + (\Delta T/T_0)}\right) \tag{16}$$

where $B = E_a/k_B$, $T = T_0 + \Delta T$.

The eq. (16) can be simplified with the following approximation.

$$\frac{1}{1 + \Delta T/T_0} \overset{\Delta T \ll T_0}{=} 1 - \Delta T \Big/ T_0 \tag{17}$$

$$D = Aexp\left(-\frac{B}{T_0} + \frac{B}{T_0^2}\Delta T\right) = Aexp\left(-\frac{B}{T_0}\right)\cdot exp\left(\frac{B}{T_0^2}\Delta T\right) \overset{\Delta T = \beta \cdot I}{=} D_0 \cdot exp(\alpha I) \tag{18}$$

where $D_0 = Aexp\left(-\frac{B}{T_0}\right)$, $\alpha = \frac{B}{T_0^2}\cdot\beta$.

Data availability

The authors do not have permission to share data.

References

[1] Manthiram A. A reflection on lithium-ion battery cathode chemistry. Nat Commun 2020;11:1550. https://doi.org/10.1038/s41467-020-15355-0.

[2] Su L, Zhang J, Huang J, Ge H, Li Z, Xie F, et al. Path dependence of lithium ion cells aging under storage conditions. J Power Sources 2016;315:35–46. https://doi.org/10.1016/j.jpowsour.2016.03.043.

[3] Su L, Zhang J, Wang C, Zhang Y, Li Z, Song Y, et al. Identifying main factors of capacity fading in lithium ion cells using orthogonal design of experiments. Appl Energy 2016;163:201–10. https://doi.org/10.1016/j.apenergy.2015.11.014.

[4] Boukoberine MN, Zhou Z, Benbouzid M. Power Supply Architectures for Drones - A Review. IECON 2019 - 45th Annu Conf IEEE Ind Electron Soc 2019;1:5826–31. https://doi.org/10.1109/iecon.2019.8927702.

[5] Liu W, Zong K, Li Y, Deng Y, Hussain A, Cai X. Nano-graphite prepared by rapid pulverization as anode for Lithium-ion batteries. Materials 2022;15:5148. https://doi.org/10.3390/ma15155148.

[6] Son D-K, Kim J, Raj MR, Lee G. Elucidating the structural redox behaviors of nanostructured expanded graphite anodes toward fast-charging and high-performance lithium-ion batteries. Carbon 2021;175:187–201. https://doi.org/10.1016/j.carbon.2021.01.015.

[7] Ding X, Zhou Q, Li X, Xiong X. Fast-charging anodes for lithium ion batteries: progress and challenges. Chem Commun 2024;60:2472–88. https://doi.org/10.1039/d4cc00110a.

[8] Gao J, Gong B, Zhang Q, Wang G, Dai Y, Fan W. Study of the surface reaction mechanism of Li4Ti5O12 anode for lithium-ion cells. Ionics 2015;21:2409–16. https://doi.org/10.1007/s11581-015-1435-x.

[9] Bernhard R, Meini S, Gasteiger HA. On-line electrochemical mass spectrometry investigations on the gassing behavior of Li4Ti5O12 electrodes and its origins. J Electrochem Soc 2014;161:A497–505. https://doi.org/10.1149/2.013404jes.

[10] Yan H, Zhu Z, Zhang D, Li W, Qilu.. A new hydrothermal synthesis of spherical Li4Ti5O12 anode material for lithium-ion secondary batteries. J Power Sources 2012;219:45–51. https://doi.org/10.1016/j.jpowsour.2012.07.023.

[11] Park H, Han DH, Goto T, Cho S, Kim W-B, Kakihana M, et al. Bottom-up method for synthesis of layered lithium titanate nanoplates using ion precursor. Chem Commun 2021;57:12536–9. https://doi.org/10.1039/d1cc03644k.

[12] Chen Y, Tao C, Lu Z, Zhang K, Liu Y, Xu G, et al. Spinel Li 4 Ti 5 O 12 hollow nanospheres prepared with colloid carbon spheres as templates for high power Li-ion battery anodes. CrystEngComm 2023;25:1090–100. https://doi.org/10.1039/d2ce01253g.

[13] Liu J, Song K, Aken Van PA, Maier J, Yu Y. Self-supported Li4Ti5O12–C nanotube arrays as high-rate and long-life anode materials for flexible Li-ion batteries. Nano Lett 2014;14:2597–603. https://doi.org/10.1021/nl5004174.

[14] Wang Y, Zhang Y, Yang W-J, Jiang S, Hou X, Guo R, et al. Enhanced rate performance of Li4Ti5O12 anode for advanced Lithium batteries. J Electrochem Soc 2019;166:A5014–8. https://doi.org/10.1149/2.0041903jes.

[15] Takami N, Inagaki H, Tatebayashi Y, Saruwatari H, Honda K, Egusa S. High-power and long-life lithium-ion batteries using lithium titanium oxide anode for automotive and stationary power applications. J Power Sources 2013;244:469–75. https://doi.org/10.1016/j.jpowsour.2012.11.055.

[16] Pasquier AD, Huang CC, Spitler T. Nano Li4Ti5O12–LiMn2O4 batteries with high power capability and improved cycle-life. J Power Sources 2009;186:508–14. https://doi.org/10.1016/j.jpowsour.2008.10.018.

[17] Svens P, Eriksson R, Hansson J, Behm M, Gustafsson T, Lindbergh G. Analysis of aging of commercial composite metal oxide – Li4Ti5O12 battery cells. J Power Sources 2014;270:131–41. https://doi.org/10.1016/j.jpowsour.2014.07.050.

[18] Belharouak I, Koenig GM, Tan T, Yumoto H, Ota N, Amine K. Performance degradation and gassing of Li4Ti5O12/LiMn2O4 Lithium-ion cells. J Electrochem Soc 2012;159:A1165–70. https://doi.org/10.1149/2.013208jes.

[19] Tong Z, Miao J, Mao J, Wang Z, Lu Y. Prediction of Li-ion battery capacity degradation considering polarization recovery with a hybrid ensemble learning model. Energy Storage Mater 2022;50:533–42. https://doi.org/10.1016/j.ensm.2022.05.026.

[20] Zhang P, Liang J, Zhang F. An overview of different approaches for battery lifetime prediction. IOP Conf Ser: Mater Sci Eng 2017;199:012134. https://doi.org/10.1088/1757-899x/199/1/012134.

[21] Epding B, Rumberg B, Jahnke H, Stradtmann I, Kwade A. Investigation of significant capacity recovery effects due to long rest periods during high current cyclic aging tests in automotive lithium ion cells and their influence on lifetime. J Energy Storage 2019;22:249–56. https://doi.org/10.1016/j.est.2019.02.015.

[22] Dubarry M, Anseán D. Best practices for incremental capacity analysis. Front Energy Res 2022;10:1023555. https://doi.org/10.3389/fenrg.2022.1023555.

[23] Dubarry M, Svoboda V, Hwu R, Liaw BY. Incremental capacity analysis and close-to-equilibrium OCV measurements to quantify capacity fade in commercial rechargeable Lithium batteries. Electrochem Solid-State Lett 2006;9:A454. https://doi.org/10.1149/1.2221767.

[24] Zhang H, Yang Y, Xu H, Wang L, Lu X, He X. Li4Ti5O12 spinel anode: fundamentals and advances in rechargeable batteries. InfoMat 2022:4. https://doi.org/10.1002/inf2.12228.

[25] Chang TC, Hasegawa K, Ibbs CW. The effects of membership function on fuzzy reasoning. Fuzzy Sets Syst 1991;44:169–86. https://doi.org/10.1016/0165-0114(91)90001-7.

[26] Bai Y, Wang D. Advanced fuzzy logic Technologies in Industrial Applications. Adv Ind Control 2006:17–36. https://doi.org/10.1007/978-1-84628-469-4_2.

[27] Safari M, Morcrette M, Teyssot A, Delacourt C. Multimodal physics-based aging model for life prediction of Li-ion batteries. J Electrochem Soc 2009;156:A145–53. https://doi.org/10.1149/1.3043429.

[28] Pinson MB, Bazant MZ. Theory of SEI formation in rechargeable batteries: capacity fade, accelerated aging and lifetime prediction. J Electrochem Soc 2013;160:A243–50. https://doi.org/10.1149/2.044302jes.

[29] Gogoana R, Pinson MB, Bazant MZ, Sarma SE. Internal resistance matching for parallel-connected lithium-ion cells and impacts on battery pack cycle life. J Power Sources 2014;252:8–13. https://doi.org/10.1016/j.jpowsour.2013.11.101.

[30] Heidrich B, Börner M, Winter M, Niehoff P. Quantitative determination of solid electrolyte interphase and cathode electrolyte interphase homogeneity in multi-layer lithium ion cells. J Energy Storage 2021;44:103208. https://doi.org/10.1016/j.est.2021.103208.

[31] Phul S, Deshpande A, Krishnamurthy B. A mathematical model to study the effect of potential drop across the SEI layer on the capacity fading of a lithium ion battery. Electrochim Acta 2015;164:281–7. https://doi.org/10.1016/j.electacta.2015.02.189.